Synthesis of the Thioborate Crystal $Zn_xBa_2B_2S_{5+x}$ ($x \approx 0.2$) for Second Order Nonlinear Optical Applications

Youngsik Kim,[†] Steve W. Martin,*[,†] Kang Min Ok,[‡] and P. Shiv Halasyamani[‡]

Department of Materials Science and Engineering, Iowa State University, Ames, Iowa 50011, and Department of Chemistry, University of Houston, Houston, Texas 77204-5641

Received September 27, 2004. Revised Manuscript Received February 18, 2005

Thioborate materials have been considered for novel infrared nonlinear optical (NLO) materials having large optical nonlinear properties combined with favorable laser damage thresholds and wide transmission ranges from the visible to the mid-infrared regions. In this work, known and new thioborate materials have been investigated that have the potential to overcome the low laser damage thresholds of the NLO chalcopyrite sulfide materials such as $AgGaS_2$ without losing their large nonlinear properties and wide transmission ranges. A new thioborate phase, polycrystalline $Zn_xBa_2B_2S_{5+x}$ ($x \approx 0.2$), has been prepared by the reaction of the metal sulfides and B_2S_3 glass in carbon crucibles sealed inside evacuated silica tubes. It crystallizes in the tetragonal system with unit cell parameters of $a = 4.762(4)$ Å and $c = 24.020(7)$ Å and is based on isolated $(BS_3)^{3-}$ structural units. The second harmonic generation (SHG) efficiency determined on powders of $Zn_xBa_2B_2S_{5+x}$ ($x \approx 0.2$) is ~50 times larger than that of α-SiO_2. The infrared spectrum shows transparency from 2.5 to 10 μm with absorption bands around 12 μm related to the vibration modes of $(BS_3)^{3-}$ units. The UV−visible spectrum shows that it is transparent in the visible region down to ~350 nm, which is a large improvement over the absorption edge of $AgGaS_2$ at 490 nm.

Introduction

Since second harmonic generation (SHG) was observed when a ruby laser was directed into a quartz crystal in 1961,[1] nonlinear optical (NLO) materials have attracted much attention owing to their use in the field of NLO devices which are now widely used in laser medicine, optical communication, and signal processing. This resulted in the development of many important nonlinear optical crystals such as $LiNbO_3$,[2−4] $KTiOPO_4$ (KTP),[5] β-BaB_2O_4 (BBO),[6−8] LiB_3O_5 (LBO),[9] and $AgGaS_2$,[10−12] to name just a few. The relationships between the chemistry, structure, and properties of NLO materials have been intensely studied to elucidate the mechanism of NLO behavior and to create new and better NLO materials.[13−16] For such purposes, the boron atom has been chosen for the central element in many NLO oxide materials. These materials have high laser damage thresholds arising from the strongly covalent B−O bonds, form large electron polarization from the planar structural units consisting of delocalized π-conjugated orbitals, and lead to a great variety in synthesizing NLO materials from various structural units.[16] With these properties, borate materials have made great progress in UV applications especially because of their high laser damage thresholds, in some cases exceeding 25 GW/cm^2, and their good UV transmission to wavelengths as low as 157 nm.[9] Typical NLO oxide materials are shown in Table 1.

Table 1. Comparison of *d*-Coefficients, Transparency, and Damage Thresholds of Selected NLO Oxide Materials

NLO material	*d*-coefficient (pm/V) at 1.064 μm	transparency (μm)	damage threshold (10^6 W/cm^2) at 1.064 μm	ref
LiB_3O_5	$d_{32} = 0.85$	0.16−2.60	25,000	9
β-BaB_2O_4	$d_{22} = 2.00$	0.20−2.60	4,500	6−8
$LiNbO_3$	$d_{31} = 4.35$	0.40−5.50	300	2−4
$LiIO_3$	$d_{31} = 4.40$	0.28−6.00	120	32, 33
KH_2PO_4	$d_{34} = 0.39$	0.17−1.57	300	4, 34

On the other hand, sulfur-based NLO materials such as $AgGaS_2$[10−12] and $CuGaS_2$,[15] which have M−S bonds and typically tetrahedral structural units, have been used for NLO applications in the IR region (2−20 μm). These infrared materials normally have larger nonlinear properties than oxide materials because of the higher polarilizability of sulfur-based bonding. However, their low laser damage thresholds arising from their small band gaps[15] limit their

* To whom correspondence should be directed. E-mail: swmartin@iastate.edu. Phone: (515) 294-0745.
[†] Iowa State University.
[‡] University of Houston.

(1) Franken, P. A.; Hill, A. E.; Peters, C. W.; Weinreich, G. *Phys. Rev. Lett.* **1961**, *7*, 118.
(2) Miller, R. C.; Nordland, W. A. *Phys. Rev.* **1970**, *B2*, 4896.
(3) Brosnan, S. J.; Byer, R. L. *IEEE J. Quantum Electron.* **1979**, *15*, 415.
(4) Dmitriev, V. G.; Gurzadyan, G. G.; Nikogosyan, D. N. *Handbook of Nonlinear Optical Crystals*; Springer: New York, 1999.
(5) Kato, K. *IEEE J. Quantum Electron.* **1991**, *27*, 1137.
(6) Chen, C.; Wu, B.; Jiang, A.; You, G. *Sci. Sinica* **1985**, *B28*, 235.
(7) Kouta, H. *Appl. Opt.* **1999**, *38* (3), 545.
(8) Bromley, L. J.; Guy, A.; Hanna, D. C. *Opt. Commun.* **1988**, *67*, 316.
(9) Chen, C.; Wu, Y. *J. Opt. Soc. Am.* **1989**, *B6*, 616.
(10) Ruderman, W.; Maffetone, J.; Zelman, D.; Poirier, D. *Mater. Res. Soc. Symp. Proc.* **1998**, *484*, 519.
(11) Bhar, G. C.; Smith, R. C. *Phys. Status Solidi* **1972**, *13*, 157.
(12) Chemla, D. S.; Kupecek, P. J.; Robertson, D. S.; Smith, R. C. *Opt. Commun.* **1971**, *3*, 29.
(13) Mei, L.; Ishizawa, N. *Rep. Res. Lab. Eng. Mater., Tokyo Inst. Technol.* **1996**, *21*, 21.
(14) Becker, P. *Adv. Mater.* **1998**, *10* (13), 979.
(15) Jackson, A. G.; Ohmer, M. C.; LeClair, S. R. *Infrared Phys. Technol.* **1997**, *38*, 233.
(16) Chen, C. T. *Development of New Nonlinear Optical Crystals in the Borate Series*; Harwood Academic Publishers: Langhorne, PA, 1993.

10.1021/cm0483083 CCC: $30.25
Published on Web 03/23/2005

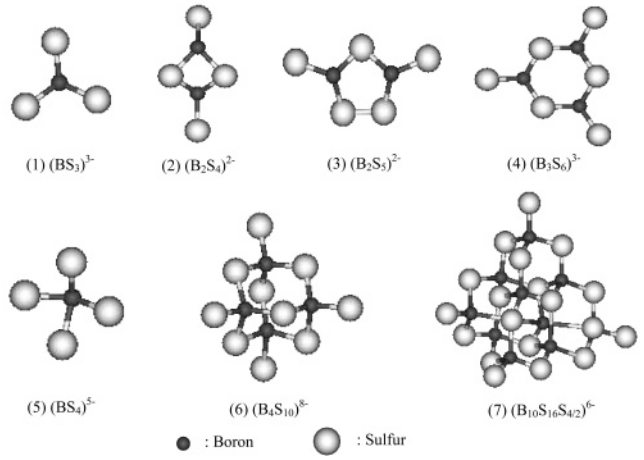

Figure 1. Various structural units in the metal thioborate crystals[18] (1) the $(BS_3)^{3-}$ unit in Li_3BS_3 and $LiSrBS_3$; (2) the $(B_2S_4)^{2-}$ unit in $Cs_2B_2S_4$; (3) the $(B_2S_5)^{2-}$ unit in $Li_2B_2S_5$ and $Na_2B_2S_5$; (4) the $(B_3S_6)^{3-}$ unit in $Na_3B_3S_6$ and $K_3B_3S_6$; (5) the isolated tetrahedral $(BS_4)^{5-}$ units have not been found in any thioborate crystal yet; (6) the macro-tetrahedra $(B_4S_{10})^{8-}$ unit in $Pb_4B_4S_{10}$; (7) the superadamantane $(B_{10}S_{16}S_{4/2})^{6-}$ unit in $Ag_6B_{10}S_{18}$, $Li_{4-2x}Sr_{2+x}B_{10}S_{19}$ ($x \approx 0.27$), $Na_6B_{10}S_{18}$.

high power application in the IR region. The search for new infrared NLO crystals with high laser damage thresholds combined with large optical nonlinearity and wide transmission ranges, visible to IR, is therefore quite active to respond to the increasing use of infrared NLO crystals in a wide range of applications such as harmonic generators, remote sensing, and molecular spectroscopy. In this research effort, thioborate materials based on boron sulfide are being considered as a new class of NLO materials by combining the favorable transparency and nonlinearity of sulfur-based NLO materials (eg., $AgGaS_2$) with the high damage thresholds of borates (eg., LiB_3O_5).

Various Structural Units of Thioborate Crystals. Metal thioborates have numerous structural units[17] that can lead to a great variation in the selection of structural types favorable to the NLO effect. For example, planar structural units containing π-conjugated orbital systems might form large electron polarization and the strong covalent B−S bonds could produce high damage thresholds. The boron atom usually coordinates with either three or four sulfide atoms to form $(BS_3)^{3-}$ or $(BS_4)^{5-}$ groups. These $(BS_3)^{3-}$ and $(BS_4)^{5-}$ units may be either isolated or connected to form planar structural units such as $(BS_3)^{3-}$, $(B_3S_6)^{3-}$, $(B_2S_4)^{2-}$, and $(B_2S_5)^{2-}$ for the former, or three-dimensional units such as $(B_4S_{10})^{8-}$ and $(B_{10}S_{16}S_{4/2})^{6-}$ for the latter, as shown Figure 1.[18] Further, many other structural units can be created through different combinations of these basic structural units. Therefore, it is expected that many different structural units of thioborate compounds can be formed and these structural units may lead to a great variation in the selection of structural types favorable for the NLO effect.

Favorable Structural Units for NLO Materials. Planar structural units such as $(BO_3)^{3-}$ and $(B_3O_6)^{3-}$ containing conjugated π-orbital systems in the borates have been found to be the most favorable structural units for NLO effect,[16] and for this reason we have explored similar thioborates containing $(BS_3)^{3-}$ and $(B_3S_6)^{3-}$ units in the search for thioborate materials with good NLO behaviors. The $2s^2$ electrons on boron atoms form planar hybridized sp^2 orbitals in $(BS_3)^{3-}$ units. These three hybridized sp^2 orbitals form three sigma bonds with three sulfur atoms, while the nonbonding p_z-orbital on each S atom is not involved in hybridization and can form a delocalized π-bonding system perpendicular to the trigonal (BS_3) plane in a way similar to that in the delocalized π-orbital system in the benzene molecule C_6H_6 and the carbonate ion CO_3^{2-}.[19] These delocalized π-orbitals are not confined just between two adjacent bonding atoms, but extend over four atoms in the BS_3 plane so that the electrons in any of these π-orbitals are able to freely move around the BS_3 plane and this delocalization produces a strong electron polarization when the electric field is applied. It is believed that this in turn is highly advantageous for large NLO coefficients.

Search for and Synthesis of Thioborates as New NLO Materials. For these reasons then, planar structural units such as $(BS_3)^{3-}$ and $(B_3S_6)^{3-}$ are expected to have large second-order susceptibilities and it should be possible to prepare new thioborate compounds containing planar structural $(BS_3)^{3-}$ and $(B_3S_6)^{3-}$ units as new NLO materials. However, compared to other inorganic compounds, metal thioborate compounds have been largely ignored because the synthesis of suitable single crystals for optical and single X-ray diffraction characterization is difficult because of the high chemical reactivity of boron sulfide.[18] So far it appears that ~34 known thioborates have been previously prepared, as shown in Table 2, and among these only three compounds, $SrLiB_3S_6$, $BaLiB_3S_6$, and $Pb_4B_4S_{10}$, appear to be noncentrosymmetric which is necessary for nonlinear optical properties. The metathioborates $SrLiB_3S_6$ and $BaLiB_3S_6$ consisting of $(B_3S_6)^{3-}$ units are extremely unstable in air because of the high content of boron sulfide and lithium sulfide, so they are not attractive candidates for new NLO materials. The relatively more stable lead thioborate $Pb_4B_4S_{10}$ consisting of $(B_4S_{10})^{8-}$ units, however, showed no SHG properties by powder SHG measurement.[20]

Therefore, the synthesis of new thioborate compounds that will have noncentrosymmetric structures with SHG properties and are reasonably stable in air are likely to be among the metal orthothioborates consisting of $(BS_3)^{3-}$ units, where chemically stable metal sulfide compounds are expected to improve the chemical stability of the boron sulfide network. These are considered to be among the best candidates for new NLO thioborates because of low symmetry, high polarizability of $(BS_3)^{3-}$ anionic groups, and smaller content of boron sulfide. In the synthesis of new thioborates for NLO materials, $XY_2(BS_3)_2$ type phases were first considered to try to avoid a center of symmetry and to improve the NLO properties by simply replacing O for S in the borate phase $XY_2(BO_3)_2$.[21−23] This simple approach has the potential to

(17) Conard, O.; Krebs, B. *Phosphorus, Sulfur, Silicon Relat. Elem.* **1997**, *124&125*, 37.
(18) Krebs, B. *Phosphorus, Sulfur, Silicon Relat. Elem.* **2001**, *168*, 11.
(19) Chang, R. *Chemistry*, 6th ed.; McGraw-Hill: Boston, MA, 1998; p 405.
(20) Kurtz, S. K.; Perry, T. T. *J. Appl. Phys.* **1968**, *39*, 3798.
(21) Smith, R. W.; Keszler, D. A. *J. Solid State Chem.* **1992**, *100*, 325.
(22) Smith, R. W.; Koliha, L. J. *Mater. Res. Bull.* **1994**, *29* (11), 1203.

Table 2. Some of the Known Thioborates, Their Crystal Systems, Point Groups, Structural Units, and Center of Symmetry

compound	crystal system	point group	space group	structural unit	center of symmetry	ref
Li_3BS_3	orthorhombic	*mmm*	*Pnma*	$(BS_3)^{3-}$		26
Na_3BS_3	monoclinic	2/*m*	*C*2/*c*	$(BS_3)^{3-}$		35
K_3BS_3	monoclinic	2/*m*	$P2_1/c$	$(BS_3)^{3-}$		35
Rb_3BS_3	monoclinic	2/*m*	$P2_1/c$	$(BS_3)^{3-}$		35
Tl_3BS_3	monoclinic	2/*m*	$P2_1/c$	$(BS_3)^{3-}$		36
$Sr_3(BS_3)_2$	monoclinic	2/*m*	*C*2/*c*	$(BS_3)^{3-}$		37
$BaLiBS_3$	monoclinic	2/*m*	$P2_1/c$	$(BS_3)^{3-}$		27
$SrLiBS_3$	orthorhombic	*mmm*	*Pnma*	$(BS_3)^{3-}$		26
$KBa_4(BS_3)_3$	monoclinic	2/*m*	*C*2/*c*	$(BS_3)^{3-}$		38
$K_4Ba_{11}(BS_3)_8S$	trigonal	$\bar{3}m$	$R\bar{3}c$	$(BS_3)^{3-}$		38
$Sr_{4.2}\ Ba_{2.8}\ (BS_3)_4S$	monoclinic	2/*m*	*C*2/*c*	$(BS_3)^{3-}$		39
$Na_3B_3S_6$	trigonal	$\bar{3}m$	$R\bar{3}c$	$(B_3S_6)^{3-}$		40
$K_3B_3S_6$	trigonal	$\bar{3}m$	$R\bar{3}c$	$(B_3S_6)^{3-}$		40
$Rb_3B_3S_6$	trigonal	$\bar{3}m$	$R\bar{3}c$	$(B_3S_6)^{3-}$		40
$Sr_3(B_3S_6)_2$	trigonal	$\bar{3}m$	$R\bar{3}c$	$(B_3S_6)^{3-}$		37
$BaLiB_3S_6$	monoclinic	*m*	*Cc*	$(B_3S_6)^{3-}$	none	27
$SrLiB_3S_6$	monoclinic	*m*	*Cc*	$(B_3S_6)^{3-}$	none	40
$Cs_2B_2S_4$	tetragonal	4/*mmm*	I_1/acd	$(B_2S_4)^{2-}$		41
$Na_2B_2S_5$	orthorhombic	*mmm*	*Pnma*	$(B_2S_5)^{2-}$		42
$Li_2B_2S_5$	orthorhombic	*mmm*	*Cmcm*	$(B_2S_5)^{2-}$		42
$K_2B_2S_7$	monoclinic	2/*m*	*I*2/*a*			43
$TlBS_3$	monoclinic	2/*m*	$P2_1/m$			44
$Tl_3B_3S_{10}$	triclinic	$\bar{1}$	$P\bar{1}$			44
$RbBS_3$	monoclinic	2/*m*	$P2_1/c$			44
SrB_2S_4	monoclinic	2/*m*	$P2_1/c$			45
$TlBS_2$	trigonal	$\bar{3}m$	$R\bar{3}m$			45
BaB_2S_4	monoclinic	*m*	*Cc*			52
$Pb_4B_4S_{10}$	tetragonal	422	$P4_12_12$	$(B_4S_{10})^{8-}$	none	46
$Li_{\ 4-2x}\ Sr_{\ 2+x}\ B_{10}S_{19}$ ($x \approx 0.27$)	monoclinic	2/*m*	$P2_1/c$	$[B_{10}S_{18}S_{2/2}]^{8-}$		47
$Ag_6B_{10}S_{18}$	monoclinic	2/*m*	*C*2/*c*	$[B_{10}S_{16}S_{4/2}]^{6-}$		48
$Na_6B_{10}S_{18}$	tetragonal	4/*mmm*	I_1/acd	$[B_{10}S_{16}S_{4/2}]^{6-}$		47
$Li_{\ 6+2x}\ [B_{10}S_{18}]S_x$ ($x \approx 2$)	monoclinic	2/*m*	*C*2/*c*	$[B_{10}S_{16}S_{\ 4/2}]^{6-}$		49
$Li_9B_{19}S_{33}$	monoclinic	2/*m*	*C*2/*c*	$[(B_{19}S_{30}S_{6/2})^{9-}]$		50
$Li_5B_7S_{13}$	monoclinic	2/*m*	*C*2/*c*	$[(B_4S_6S_{4/2})^{4-}\ (B_{10}S_{16}S_{4/2})^{6-}]$		50

synthesize noncentrosymmetric thioborates because, as shown above, borates and thioborates share many of the same structures.

The synthesis of various new polycrystalline orthothioborates of general formula $XY_2(BS_3)_2$, where X and Y are different cations with +2 formal charges, (XY_2 = $BaZn_2$, $ZnBa_2$, $BaCu_2$, $CuBa_2$, $CuSr_2$, $SrCu_2$, $SrPb_2$, $PbSr_2$, $PbZn_2$, $ZnPb_2$, $BaPb_2$, $PbBa_2$) have been tried. From all of this effort, we report a new thioborate polycrystalline $Zn_xBa_2B_2S_{5+x}$ ($x \approx 0.2$) phase that was initially batched to yield the orthothioborate phase $Ba_2Zn(BS_3)_2$. Upon careful inspection and compositional analysis it was found that $x \approx 0.2$ for this phase and is not the expected $x = 1$ value. We report the synthesis, structural characterization, and nonlinear optical properties of this phase.

Experimental Section

Synthesis. High-purity glassy B_2S_3 was prepared from amorphous boron (99.9% metal basis, Cerac) and sulfur (99.999%, Cerac) using a procedure modified from literature[24] and was used as the starting material for B_2S_3. Powders of $Zn_xBa_2B_2S_{5+x}$ ($x = 0$, 0.15, 0.2, 0.4, 1) were prepared from 1-g batches of the stoichiometric amounts of the starting compounds, BaS (Cerac, 99.9%), ZnS(Fisher Scientific, 99.99%), and B_2S_3. They were mixed and then pre-reacted by placing the starting materials in a covered vitreous carbon crucible and heated for 15 min at 900 °C inside a mullite tube lined muffle furnace attached hermetically to the side of a high-quality oxygen- and water-free glovebox (<5 ppm O_2 and <5 ppm H_2O). The sample was cooled to room temperature in the carbon crucible in the glovebox, ground to a fine powder, and then heated again for 15 min at 900 °C. After regrinding, the product was placed into a vitreous carbon crucible, and then placed inside a predried silica tube and sealed under vacuum. The sealed tube and contents were heated according to the temperature profile shown as eq 1. Light yellow to white powders were obtained when the samples were ground. The samples of $Zn_xBa_2B_2S_{5+x}$ ($x = 0.15$, 0.2, 0.4, 1) phases are relatively stable in air (exposure to air for 4 h did not change the XRD powder pattern). However, as a precaution all samples were handled in a dry helium glovebox.

$$\text{RT} \xrightarrow{5\text{ h}} 900\ ^\circ\text{C (24 h)} \xrightarrow{3.4\text{ h}} 700\ ^\circ\text{C (10 h)} \xrightarrow{12\text{ h}} 600\ ^\circ\text{C (24 h)} \xrightarrow{35\text{ h}} 500\ ^\circ\text{C (24 h)} \xrightarrow{1\text{ h}} 450\ ^\circ\text{C} \xrightarrow{\text{quench}} \text{RT} \quad (1)$$

Powder X-ray Diffraction. The powder X-ray diffraction data for finely ground (<20 μm) $Zn_xBa_2B_2S_{5+x}$ ($x = 0$, 0.15, 0.2, 0.4, 1) phases were collected at 298 K on a Scintag XDS2000 diffractometer using Cu Kα radiation (λ = 1.5406 Å). It was operated at 40 kV and 30 mA in the 2θ range of 13−80° in step scan mode with step size 0.02° and step time 6.0 s. The cell constants of the $Zn_xBa_2B_2S_{5+x}$ ($x \approx 0.2$) phase were obtained by using the software DICVOL91,[25] and the unit cell, d_{obs}, d_{calc}, and I(%) values are listed in Table 3.

(23) Ji, Y.; Liang, J.; Xie, S.; Yu, Y. *J. Am. Ceram. Soc.* **1995**, *78* (3), 765.
(24) Martin, S. W.; Bloyer, D. R. *J. Am. Ceram. Soc.* **1990**, *73*, 3481.
(25) Boultif, A.; Louer, D. *J. Appl. Crystallogr.* **1991**, *24*, 987.

Table 3. Powder XRD Data for $Zn_xBa_2B_2S_{5+x}$ ($x \approx 0.2$); Tetragonal System, $a = 4.762(4)$ Å, and $c = 24.020(7)$ Å

h	*k*	*l*	d_{obs}	d_{cal}	*I*(%)
0	0	4	6.005	6.005	6
1	0	1	4.671	4.672	80
1	0	3	4.093	4.093	4
0	0	6	4.002	4.003	42
1	0	5	3.382	3.382	91
1	1	0	3.367	3.368	71
1	1	2	3.242	3.243	13
0	0	8	3.002	3.003	6
1	1	4	2.937	2.937	2
1	0	7	2.784	2.784	51
1	1	6	2.577	2.577	100
0	0	10	2.401	2.402	4
1	1	7		2.404	0
2	0	0	2.381	2.381	40
1	0	9	2.328	2.328	3
2	1	1	2.121	2.122	15
2	0	6	2.046	2.047	26
0	0	12	2.001	2.002	13
1	0	11	1.985	1.985	17
2	1	5	1.947	1.947	3
2	1	7	1.809	1.810	4
1	0	13	1.722	1.723	3
0	0	14	1.716	1.716	0
2	0	10	1.691	1.691	4
2	2	0	1.684	1.684	8
2	1	9	1.664	1.665	1
2	2	4	1.621	1.621	4
2	2	6	1.552	1.552	13
2	0	12	1.532	1.532	9
2	1	11	1.524	1.525	10
2	1	11	1.525	1.525	6
3	0	5	1.507	1.507	11
3	1	0	1.506	1.506	10
3	0	7	1.441	1.441	6
3	1	6	1.409	1.410	6
2	1	13	1.395	1.396	3
1	1	16	1.371	1.371	2
1	0	17	1.355	1.355	8
0	0	18	1.335	1.334	3
3	2	1	1.319	1.319	2
3	2	3	1.303	1.303	0
2	2	12	1.289	1.289	4
3	0	11	1.284	1.284	2
2	1	15	1.280	1.280	1
3	1	10	1.276	1.276	0
3	2	5	1.274	1.274	2
1	1	18	1.241	1.241	23
3	2	7	1.233	1.233	3

Infrared (IR) Spectroscopy. The mid-infrared spectra were recorded in the range of 4000−400 cm^{-1} with the use of a Bruker IFS 66v/S spectrometer on samples using the KBr pellet method. Samples of 2 mg were ground with 100 mg of KBr, previously dried at 300 °C, and pressed into pellets. The IR transmission spectra typically were obtained using 32 scans at 4 cm^{-1} resolution.

UV/VIS/NIR Spectroscopy. The UV/VIS/NIR spectra were recorded in the range of 200−3000 nm at room temperature using a PE Lambda-19 spectrometer. The UV/VIS/NIR spectra of the samples were taken using the KBr pellet method. 2 mg of the samples were ground with 100 mg of KBr, previously dried at 300 °C, and pressed into pellets for transmission.

Second-Harmonic Generation Measurements. The second-order nonlinearity of powder samples of $Zn_xBa_2B_2S_{5+x}$ ($x \approx 0.2$) have been examined using a modified Kurtz-NLO system with a 1064 nm Nd:YAG laser.[20] The polycrystalline samples and α-SiO_2-(reference) were ground to powders (45−63 μm) and were placed in separate capillary tubes. The sample was irradiated with a Nd:YAG laser (1064 nm) and the filtered SHG light, 532 nm, was collected in reflection and detected by a photomultiplier tube (Oriel Instruments). A digital oscilloscope (Tektronix TDS 3032) was used to display the SHG signal. The powder SHG properties of the samples were expressed as the comparative intensity [$I^{2w}/I^{2w}_{(SiO2)}$] of α-SiO_2.

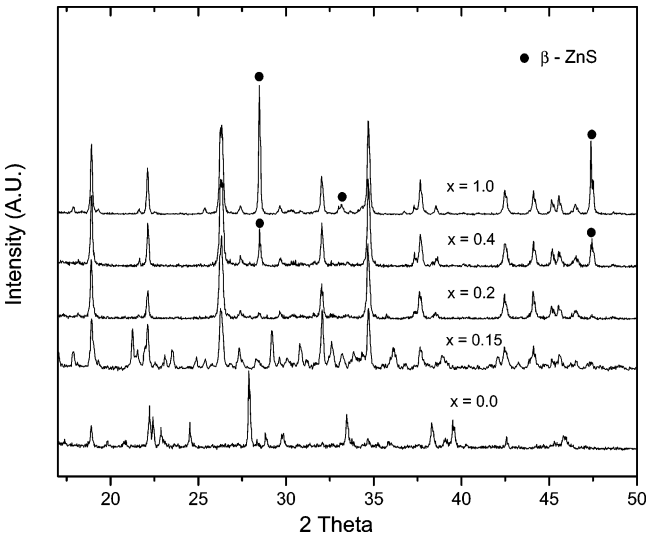

Figure 2. Powder X-ray diffraction patterns of the $Zn_xBa_2B_2S_{5+x}$ ($x = 0$, 0.15, 0.2, 0.4, 1) phases. X-ray peaks of β-ZnS appeared in the $Zn_xBa_2B_2S_{5+x}$ ($x = 0.4$, 1) phase, but the intensity decreased with low content of ZnS. Eventually, no β-ZnS peaks appeared in the $Zn_xBa_2B_2S_{5+x}$ ($x = 0.2$).

Results and Discussion

Powder X-ray Diffraction Measurements. The synthesis of the orthothioborate phase $Zn_xBa_2B_2S_{5+x}$ ($x = 1$) was tried initially, but powder X-ray diffraction patterns revealed that this composition phase separated into β-ZnS and a second phase, later identified as $Zn_xBa_2B_2S_{5+x}$ ($x \approx 0.2$) as shown in Figure 2. The structure of the $Zn_xBa_2B_2S_{5+x}$ ($x \approx 0.2$) phase has been indexed by the DICVOL91 program.[25] The powder X-ray diffraction data in the 2θ range of 13−80° were indexed. This phase could be indexed as a tetragonal structure with the lattice constant $a = 4.762(4)$ Å and $c = 24.020(7)$ Å as shown in Table 3. The systematic extinction of the diffraction lines indicates that the possible space group of this compound is *I*4, $I\bar{4}$, *I*4/*m*, *I*422, *I*4*mm*, $I\bar{4}2m$, $I\bar{4}m2$, or *I*4/*mmm*. Among those, *I*4/*m*, *I*422, and *I*4/*mmm* are centric structures and were eliminated because they are inconsistent with the result of the powder SHG test. Therefore, the possible space group is one of the following five space groups: *I*4, $I\bar{4}$, *I*4*mm*, $I\bar{4}2m$, and $I\bar{4}m2$.

To further resolve the structure of this phase, the synthesis of suitable single crystals of $Zn_xBa_2B_2S_{5+x}$ ($x \approx 0.2$) for single X-ray diffraction was attempted, but even with using many different heating and slow cooling schedules, sufficiently large crystals (∼0.1 mm) could not be prepared. However, in one instance a yellowish tiny crystal of poor quality was obtained and that was later found to also be badly twinned. Single-crystal X-ray diffraction measurements of this crystal suggested the tetragonal system with $a = 4.763$ Å and $c = 24.027$ Å (comparable with $a = 4.762(4)$ Å and $c = 24.020(7)$ Å determined from powder X-ray diffraction) and the most possible space group was determined to be $I\bar{4}2m$. Unfortunately, further investigation of the structure was not possible using this poor quality crystal.

Infrared and UV/VIS/NIR Absorption. To further characterize the structure of the phase, the structurally known

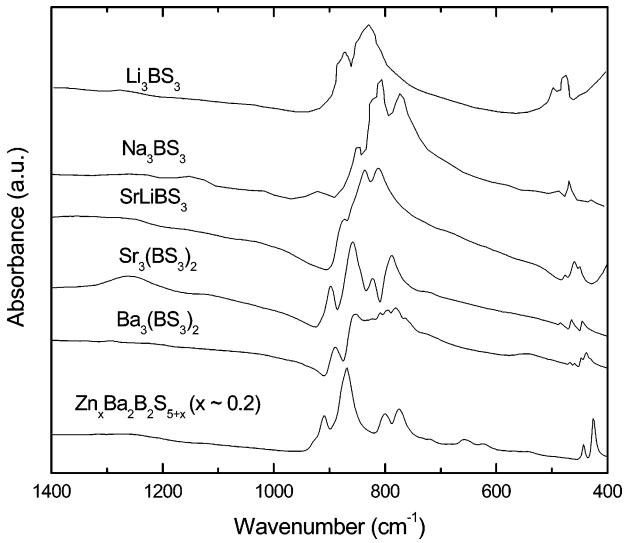

Figure 3. IR spectra of various orthothioborate compounds consisting of isolated trigonal planar $(BS_3)^{3-}$ units. The main absorption bands ~850 cm^{-1} arise from the asymmetric stretches modes of the $(BS_3)^{3-}$ unit. Weak absorption bands ~450 cm^{-1} assigned to the symmetric stretches modes of $(BS_3)^{3-}$ unit. The different peak frequency of the mode for each phase would be expected from the different mass of the metal counterion in these phases.

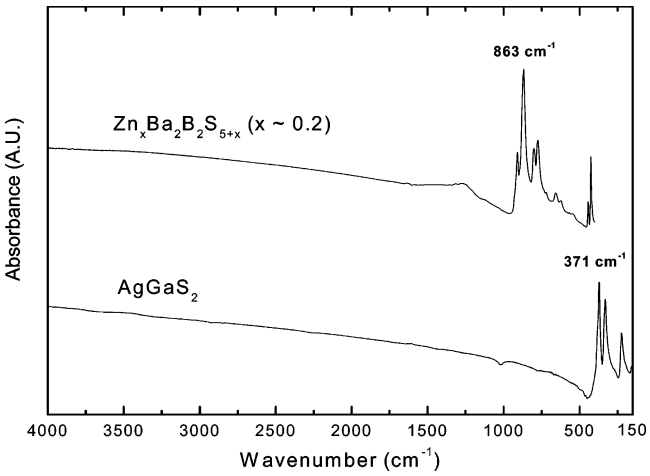

Figure 4. Infrared spectra of $Zn_xBa_2B_2S_{5+x}$ ($x \approx 0.2$) and $AgGaS_2$ powder suspended in a KBr matrix. The main absorption bands around 850 cm^{-1} are assigned to the vibration mode of $(BS_3)^{3-}$ unit and indicate that the IR absorption edge of this material may lie below 1000 cm^{-1} (10 μm), so it can be transparent until 10 μm.

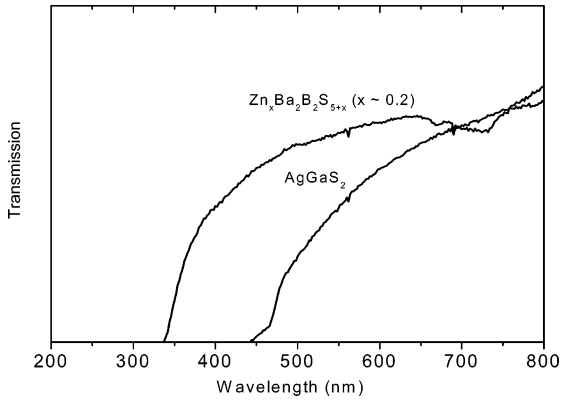

Figure 5. UV/VIS transmission spectra of $Zn_xBa_2B_2S_{5+x}$ ($x \approx 0.2$) and $AgGaS_2$ powders measured in a KBr pellet. $Zn_xBa_2B_2S_{5+x}$ ($x \approx 0.2$) has a shorter absorption edge (~350 nm) than that (~490 nm) of $AgGaS_2$, which makes it have a higher damage threshold.

orthothioborates such as Li_3BS_3, $SrLiBS_3$, and $Sr_3(BS_3)_2$ consisting of isolated $(BS_3)^{3-}$ units have been prepared, and the IR spectra of these compounds were compared to that of $Zn_xBa_2B_2S_{5+x}$ ($x \approx 0.2$) and are shown in Figure 3. In the IR spectra of $SrLiBS_3$[26] and $BaLiBS_3$[27] crystals, strong absorption bands occur around 850 cm^{-1} and weak absorption bands occur around 450 cm^{-1}; these are assigned to the asymmetrical stretching E modes and the symmetrical stretching A_1' modes of the $(BS_3)^{3-}$ unit, respectively, in the point symmetry group of D_{3h}. These two absorption bands are also observed in IR spectra of the alkali orthothioborates, M_3BS_3 (M = Li, Na, K, Rb, and Cs).[28] The IR absorption spectrum of $Zn_xBa_2B_2S_{5+x}$ (x ~ 0.2) is very similar to those of the other orthothioborate crystals and shows strong absorption bands from 907 to 778 cm^{-1} and weak absorption bands at 444 and 425 cm^{-1} which can be assigned to the asymmetrical stretching modes and the symmetrical stretching modes of the orthothioborate $(BS_3)^{3-}$ unit, respectively. These assignments strongly suggest that the $Zn_xBa_2B_2S_{5+x}$ ($x \approx 0.2$) phase consists of isolated trigonal planar $(BS_3)^{3-}$ units like the other orthothioborates. Additional absorption bands are not observed in the mid-IR range, and for this reason the $Zn_xBa_2B_2S_{5+x}$ ($x \approx 0.2$) phase may be expected to be transparent in the mid-IR range down to ~1000 cm^{-1} (10 μm) as shown the Figure 4. In addition, Figure 5 shows that it is transparent in the visible region down to ~350 nm, where the improved visible transparency is compared to that of $AgGaS_2$. Since the absorption edge is closely related to the band gap and the damage thresholds of optical materials,[29] the approximate damage thresholds can be obtained from measurement of the absorption edges. The band gap of $Zn_xBa_2B_2S_{5+x}$ ($x \approx 0.2$) is estimated at ~3.5 eV, which is not only higher than that of $AgGaS_2$ and $AgAsS_3$ but also higher than $LiNbO_3$, and these values are listed in Table 4.

Second-Order NLO Properties and Damage Threshold. Powder SHG measurements of the $Zn_xBa_2B_2S_{5+x}$ ($x \approx 0.2$) phase were performed to determine its NLO SHG behavior. These experiments revealed that $Zn_xBa_2B_2S_{5+x}$ ($x \approx 0.2$) had a SHG efficiency of ~50 times greater than that of powder samples of α-SiO_2. This SHG response further confirmed that $Zn_xBa_2B_2S_{5+x}$ ($x \approx 0.2$) phase belongs to a noncentrosymmetric space group.

To examine the laser damage threshold of this phase, a qualitative test was performed. Single laser shots from the Nd:YAG laser revealed that $Zn_xBa_2B_2S_{5+x}$ ($x \approx 0.2$) was not damaged under prolonged laser irradiation as evidenced by the continued strong production of 532-nm light. $AgGaS_2$ (a typical infrared NLO material), on the other hand, immediately decomposed (darkened) after showing low intensity of SHG ($1 \times I^{2w}_{SiO2}$) and then eventually even this SHG intensity disappeared completely. At the same laser wavelength, a low SHG signal from α-Pb_2GeS_4 ($0.2 \times I^{2w}_{SiO2}$) has been previously reported,[30] but an isostructural compound, $Na_{0.5}Pb_{1.75}GeS_4$, showed a higher SHG intensity

(26) Hiltmann, F.; Jansen, C.; Krebs, B. *Z. Anorg. Allg. Chem.* **1996**, *622*, 1508.
(27) Hiltmann, F.; Krebs, B. *Z. Anorg. Allg. Chem.* **1995**, *621*, 424.
(28) Cho, J.; Martin, S. W. *J. Non-Cryst. Solids* **2002**, *298*, 176.
(29) Wu, K. Chen, C. T. *Appl. Phys.* **1992**, *A54*, 209.

Table 4. Comparison of the Absorption Edges and Damage Thresholds in the Selected NLO Materials[a]

compound	anionic group	absorption edge (um)	energy gap (eV)	damage threshold (MW/cm^2) at $\lambda = 1.064\ \mu m$	ref
$Zn_xBa_2B_2S_{5+x}$ ($x \approx 0.2$)	(BS_3)	0.35	3.54		
$LiNbO_3$	(NbO_6)	0.4	3.50	300	2−4
$AgGaS_2$	(GaS_4)	0.50	2.62	20	10−12
Ag_3AsS_3	(AsS_3)	0.55	2.00	10	4, 15, 51

[a] The absorption edges are closely related to the energy gap and damage thresholds (the shorter the absorption edges, the higher the damage threshold). $Zn_xBa_2B_2S_{5+x}$ ($x \approx 0.2$) may have a high damage threshold among the sulfur-based NLO materials due to strongly covalent bonded $(BS_3)^{3-}$ anions.

$(7-8 \times I^{2w}_{LiNbO3})$ from a 3.5-μm laser.[31] Therefore, these sulfide NLO materials have been used in infrared applications but may not be useful for 1.064-μm laser applications due to their low energy band gap. The strong SHG intensity from $Zn_xBa_2B_2S_{5+x}$ ($x \approx 0.2$) indicates that this phase may be useful for both 1.064 μm and large wavelength infrared application.

The high laser damage thresholds of the $Zn_xBa_2B_2S_{5+x}$ ($x \approx 0.2$) phase can be expected from the $(BS_3)^{3-}$ anionic groups in this phase because the absorption edges of the inorganic crystals can be determined by the localized molecular orbitals of the anionic groups.[29] In the borate crystals, larger anionic groups containing the smaller tetrahedral $(BO_4)^{5-}$ group such as $(B_3O_9)^{9-}$ and $(B_3O_7)^{5-}$ have higher damage thresholds than the planar $(BO_3)^{3-}$ and $(B_3O_6)^{3-}$ anionic groups because these latter planar anionic groups contain π-conjugated orbitals, which create smaller energy band gaps.[16] However, borate crystals containing the borate groups composed of planar anionic groups have much higher damage thresholds than that of the other oxide NLO materials such as $LiNbO_3$, $LiIO_3$, and KH_2PO_4 because of the strong covalent bonding of boron atoms in the $(BO_3)^{3-}$ anionic group, see Table 1. While it is expected that $Zn_xBa_2B_2S_{5+x}$ ($x \approx 0.2$) will have a lower damage threshold than those of phases containing $(BO_3)^{3-}$ units, compared to other NLO sulfide-based materials such as $AgGaS_2$, $AgAsS_3$, and $HgGa_2S_4$, $Zn_xBa_2B_2S_{5+x}$ ($x \approx 0.2$) containing covalent bonded $(BS_3)^{3-}$ anions has a shorter absorption edge (larger band gap) and this will induce a higher laser damage threshold, see Table 4. Therefore, such NLO thioborates can improve upon the critical drawback of the sulfide-based NLO materials, a low laser damage threshold, without losing their advantages of high nonlinear properties and wide transparency range.

Summary and Conclusions

Metal thioborates consisting of the trigonal planar $(BS_3)^{3-}$ structural unit have been investigated as new NLO materials because the planar $(BS_3)^{3-}$ unit containing conjugated π-orbital systems will produce high nonlinear optical properties, and the strongly covalent bonding of boron atoms in the $(BS_3)^{3-}$ anionic group will enable high damage thresholds and a wide transparency range from the visible to mid-IR regions. A $Zn_xBa_2B_2S_{5+x}$ ($x \approx 0.2$) phase crystallized in the noncentrosymmetric tetragonal space group $I\bar{4}2m$ with lattice constants $a = 4.762(4)$ Å and $c = 24.020(7)$ Å, and consists of the trigonal planar $(BS_3)^{3-}$ structural units. $Zn_xBa_2B_2S_{5+x}$ ($x \approx 0.2$) yields strong SHG effects about 50 times greater than that of α-SiO_2 and has a wide transparent range from the visible to the mid-IR region (0.35−10 μm). Additionally, an absorption edge estimation supports its much higher laser damage threshold than that of other sulfur-based NLO materials. While the $Zn_xBa_2B_2S_{5+x}$ ($x \approx 0.2$) phase is the first such NLO thioborate phase to be discovered, many other metal thioborates are possible and may yield a number of excellent candidate materials that have high nonlinear optical properties combined with wide transmission and high damage thresholds for second-order NLO application in both the visible and IR regions.

Acknowledgment. Funding of this work was provided by the Iowa State University Carver Trust Grant and the NSF under grant 99-724660. Work at the University of Houston was supported in part by the Welch Foundation and NSF-DMR 0092054.

CM0483083

(30) Poduska, K. M.; Cario, L. DiSalvo, F. J.; Min, K.; Halasyamani, P. S. *J. Alloys Compd.* **2002**, *335*, 105.
(31) Aitken, J. A.; Marking, G. A.; Evain, M.; Iordanidis, L.; Kanatzidis, M. G. *J. Solid State Chem.* **2000**, *153*, 158.
(32) Kato, K. *IEEE J. Quantum Electron.* **1985**, *21*, 119.
(33) Nath, G.; Haussuhl, S. *Appl. Phys. Lett.* **1969**, *14*, 154.
(34) Hagen, W. F.; Magnante, P. C. *J. Appl. Phys.* **1969**, *40*, 219.
(35) Kuchinke, J.; Jansen, C.; Lindemann, A.; Krebs, B. *Z. Anorg. Allg. Chem.* **2001**, *627*, 896.
(36) Krebs, B.; Hamann, W. *J. Less-Common Met.* **1988**, *137*, 143.
(37) Hammerschmidt, A.; Doech, M.; Püttmann, C.; Krebs, B. *Z. Anorg. Allg. Chem.* **2003**, *629* (3), 551.
(38) Hammerschmidt, A.; Jansen, C.; Küper, J.; Köster, C.; Krebs, B. *Z. Anorg. Allg. Chem.* **2001**, *627*, 669.
(39) Hammershmidt, A.; Köster, C.; Küper, J.; Lindemann, A.; Krebs, B. *Z. Anorg. Allg. Chem.* **2001**, *627*, 1253.
(40) Püttmann, C.; Diercks, H.; Krebs, B. *Phosphorus, Sulfur, Silicon Relat. Elem.* **1992**, *65*, 1.
(41) Hammerschmidt, A.; Jansen, C.; Küper, J.; Püttmann, C.; Krebs, B. *Z. Anorg. Allg. Chem.* **1995**, *621*, 1330.
(42) Jansen, C.; Küper, J.; Krebs, B. *Z. Anorg. Allg. Chem.* **1995**, *621*, 1322.
(43) Hammerschmidt, A.; Küper, J.; Stork, L.; Krebs, B. *Z. Anorg. Allg. Chem.* **1994**, *620*, 1898.
(44) Püttmann, C.; Hiltmann, F.; Hamann, W.; Brendel, C.; Krebs, B. *Z. Anorg. Allg. Chem.* **1993**, *619*, 109.
(45) Püttmann, C.; Hamann, W.; Krebs, B. *J. Solid State Inorg. Chem.* **1992**, *29*, 857.
(46) Hardy, A. *Bull. Soc. Miner. Cristallogr.* **1968**, *91*, 111.
(47) Hammerchmidt, A.; zum Hebel, P.; Hiltmann, F.; Krebs, B. *Z. Anorg. Allg. Chem.* **1996**, *622*, 76.
(48) Krebs, B.; Diercks, H. *Z. Anorg. Allg. Chem.* **1984**, *518*, 101.
(49) zum Hebel, P.; Krebs, B.; Grüne, M.; Müller-Warmuth, W. *Solid State Ionics* **1990**, *43*, 133.
(50) Hiltmann, F.; Hebel, P.; Hammerschmidt, A.; Krebs, B. *Z. Anorg. Allg. Chem.* **1993**, *619*, 293.
(51) Hulme, K. F.; Jones, O.; Davies, P. H.; Hobden, M. V. *Appl. Phys. Lett.* **1967**, *10*, 133.
(52) Hammerschmidt, A.; Döch, M.; Wuff, M.; Krebs, B. *Z. Anorg. Allg. Chem.* **2002**, *628*, 2637.